

Crystal Structure of High Temperature Phase and Ionic Conductivity Mechanism of CuHgSX (X = Cl, Br)

Masakazu Moro'oka,* Hiroshi Ohki, Koji Yamada, and Tsutomu Okuda

Department of Chemistry, Graduate School of Science, Hiroshima University,
1-3-1 Kagamiyama, Higashi-Hiroshima, Hiroshima 739-8526

Received April 14, 2003; E-mail: morooka@hiroshima-u.ac.jp

We found a new ionic conduction phase in CuHgSCl above 373 K and in CuHgSBr above 346 K. The crystal structures of these novel phases have been determined by Rietveld refinement of powder X-ray diffraction patterns. The electric conductivity at 500 K measured by AC impedance method was 1.4×10^{-5} S cm^{-1} for CuHgSCl and 4.0×10^{-6} S cm^{-1} for CuHgSBr. The activation enthalpy was determined to be 53 kJ mol^{-1} for CuHgSCl and 67 kJ mol^{-1} for CuHgSBr. The ionic transport number measurements indicated that Cu^+ ions constitute the majority charge carriers in these samples. The electronic contribution to the conduction process is small in comparison with the Cu^+ ionic contribution. The charge density analysis by the maximum entropy method (MEM) combined with Rietveld analysis clearly showed that the Cu^+ ionic conduction path was along the crystallographic (100) direction.

It is well known that copper and silver halogenides are cationic conductors. Many double salts of these halogenides with other compounds show higher conductivity at lower temperature. For example, Cu_2HgI_4 and Ag_2HgI_4, which are synthesized by the reaction of CuI or AgI with HgI_2, undergo phase transitions at 342 K and 323 K, respectively, and the electric conductivity σ jumps one to two orders of magnitude.

In the family of MHgSX (M = Cu, Ag; X = Cl, Br, I), which were prepared by combination of copper and silver halogenides with HgS, only a few compounds have been characterized. Gullio et al. determined the crystal structures of CuHgSCl and CuHgSBr.[1] They showed the electrical conductivity and activation energy only at 298 K for CuHgSBr. Blachnik et al. synthesized AgHgSBr and AgHgSI, and made a phase diagram of the AgI–HgS system.[2] They synthesized AgHgSCl and examined the equilibrium diagrams of the CuCl–HgS and AgCl–HgS systems as well.[3] On the other hand, Beck et al. reported the structures of CuHgSeBr, AgHgSBr and AgHgSI synthesized by hydrothermal synthesis.[4] Recently, they reported new structures of CuHgSCl and CuHgSBr, which are different from those given by Gullio et al.[5]

In this paper, we report the conductivity and the mechanism for the high temperature phases of CuHgSCl and CuHgSBr. These compounds were easily synthesized by solid-state reaction. Although the structure of the high temperature phase of CuHgSBr was determined by Beck et al., the structure and the phase transition temperature for CuHgSCl are unknown. Therefore, we have determined the structure of CuHgSCl by Rietveld refinement of powder X-ray diffraction pattern. Moreover, the Cu^+ ion behavior at high temperatures was studied by maximum entropy method (MEM)/Rietveld method. We will discuss the ion conduction mechanism for CuHgSX (X = Cl, Br).

Experimental

CuHgSX (X = Cl, Br) were prepared by heating stoichiometric mixtures of CuX (Kojundo Chemical Lab. Co.) and red-HgS (Kojundo Chemical Lab. Co.) in an evacuated Pyrex tube at ca. 573 K for 2 weeks. CuX was synthesized by a solid-state reaction between CuX_2 (Kojundo Chemical Lab. Co.) and powdered Cu metal (Soekawa Chemicals Co.).

Differential thermal analysis (DTA) measurements were carried out by use of a homemade apparatus. The powder X-ray diffraction patterns were measured on a Rigaku Rint 2000 system using Cu-Kα radiation with scan rate = 0.5 degree/min and scan step of 0.02 degree.

The crystal structure of the high temperature phase was initially guessed by the Monte Carlo Method,[6] and refined by Rietveld method using the RIETAN2000 program.[7]

The electron densities of these crystals were analyzed by Maximum Entropy Method (MEM) combined with the Rietveld pattern fitting.[8] During the electron density analysis, the unit cell of the sample was divided into edges of ca. 0.1 Å each.

The electric conductivity was determined by AC impedance method. The complex impedance measurements were performed by the two-terminal method using a computer-interfaced HIOKI 3532 LCR meter (42 Hz–5 MHz). The pellet sizes were 13 mm diameter and 1.5–1.8 mm thickness. Carbon paint was applied on both sides of the pellet and electrodes to insure a good contact with each other. The temperature of the sample was controlled within $\pm$1 K using a Chino KP1000 temperature controller equipped with Cu–Constantan thermocouples.

The ionic transport measurements were carried out using an ion-blocking method and a non-blocking method. (i) In the non-blocking method, the two pellets of the sample were sandwiched between copper electrodes. A constant DC current of 0.01 mA was applied across the sample for 5 days at 500 K using an ADVANTEST programmable DC voltage/current generator. (ii) In the ion-blocking method, the two pellets of the sample were sand-

Published on the web November 15, 2003; DOI 10.1246/bcsj.76.2111

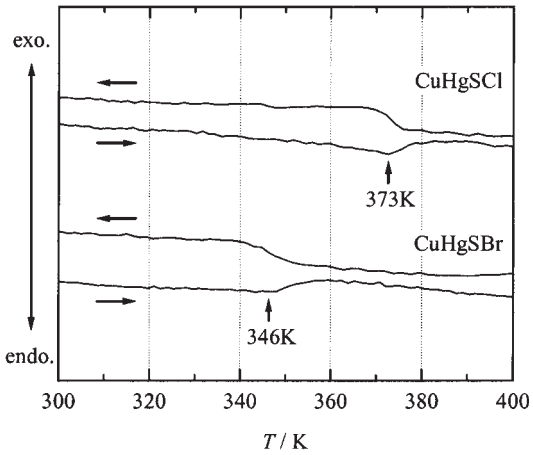

Fig. 1. The DTA curves of CuHgSX (X = Cl, Br).

Table 1. Experimental Conditions and Crystallographic Data for CuHgSCl at 400 K

Compound	CuHgSCl
Space group	*Pmam* (No. 51)
Crystal system	Orthorhombic
Color	Orange
Lattice constants/Å	$a = 9.8870(3)$ $b = 8.8554(3)$ $c = 4.1036(1)$
Volume/Å^3	359.29(2)
d_{cal}/g cm^{-3}	6.13
Z	4
Range 2θ/°	5–100
Scan step/°	0.02
R_p/%	3.54
R_{wp}/%	4.62
R_{exp}/%	3.12
R_{Bragg}/%	4.10
S	1.48

Table 2. Positional Parameters of CuHgSCl at 400 K

Atom	Position	x	y	z	U_{iso}/Å^2
Cu	4(i)	0.0825(3)	0.3032(3)	0	0.079(1)
Hg1	2(b)	1/2	1/2	1/2	0.0433(6)
Hg2	2(d)	1/4	0.7172(2)	1/2	0.0323(6)
S	4(j)	0.0072(4)	0.7238(5)	1/2	0.026(2)
Cl1	2(e)	1/4	0.0495(7)	0	0.044(2)
Cl2	2(e)	1/4	0.4743(7)	0	0.032(2)

wiched between copper electrodes with carbon paint on both sides of the pellets. A constant DC voltage of 10 V was applied across the sample for 3 days at room temperature using an ADVANTEST programmable DC voltage/current generator.

Results

DTA. Figure 1 shows the DTA curves for CuHgSX (X = Cl, Br). For CuHgSCl, an endothermic peak appeared at 373 K on heating and an exothermic one at the same temperature on cooling. As for CuHgSBr, endothermic and exothermic peaks were seen at 346 K on both heating and cooling processes. The thermal decomposition takes place above 727 K for CuHgSCl and above 627 K for CuHgSBr.

Rietveld Analysis. Figure 2 shows the result of the Rietveld refinement using powder X-ray diffraction patterns of CuHgSCl at 400 K. The space group and the lattice parameters are summarized in Table 1 along with the refinement conditions. Table 2 lists the atomic positions and the isotropic thermal parameters determined through the refinement, while Table 3 shows the selected interatomic bond distances and angles. Figure 3 depicts the crystal structures in the low and high temperature phases of CuHgSCl.

MEM Analysis. Figure 4 shows the electron density maps along (001) plane for CuHgSCl at room temperature. The electron distribution on each atom is shown. The contour lines were drawn in log scale intervals. Figure 5 indicates the charge density map at 500 K.

The electron density maps for CuHgSBr are deduced and the results at room temperature and 500 K are shown in Figs. 6 and 7, respectively.

Table 3. Interatomic Distance (Å) and Bond Angles (°) in CuHgSCl at 400 K

Cu–X1	2.787(2)
Cu–X2	2.252(2)
Cu–S	2.246(3)
Hg1–X2	2.974(3)
Hg1–S	2.404(2)
Hg2–X1	3.242(3)
Hg2–S	2.442(2)
S–Cu–S	131.9(4)
X1–Cu–X2	96.2(1)
S–Hg1–S	177.0(4)
S–Hg2–S	180

Conductivity. Figure 8 represents the electric conductivity plotted against the inverse temperature for CuHgSX. With increasing temperature, the conductivity increased monotonously. For CuHgSCl, no obvious change was observed at the phase transition temperature. From the slopes of these curves, the activation enthalpies for conduction were determined to be 53 kJ mol^{-1} for CuHgSCl and 67 kJ mol^{-1} for CuHgSBr.

Ionic Transport. The measurements by non-blocking method indicate that Cu^+ ions constitute the majority charge carriers in these samples. A copper metallic luster was separated out in between sample and electrode. Moreover, the ionic

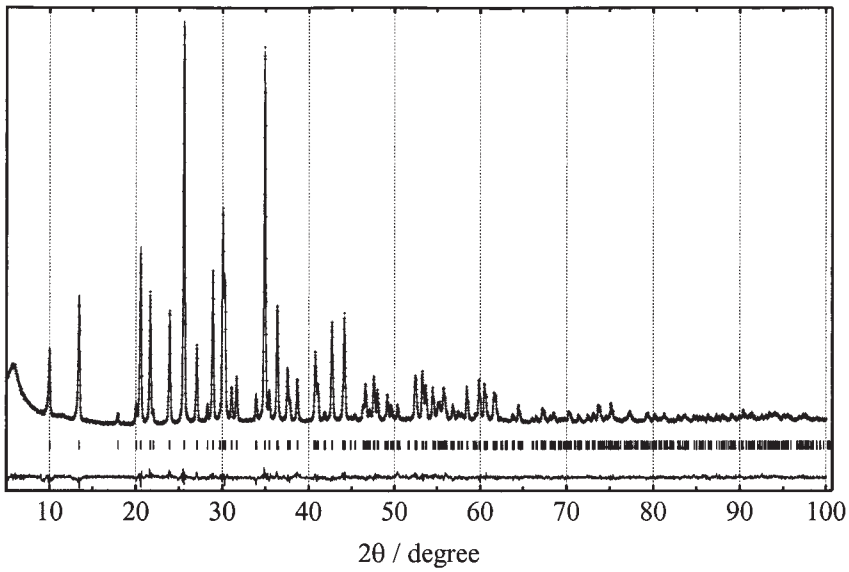

Fig. 2. Observed (cross) and calculated (solid line) X-ray diffraction pattern of CuHgSCl at 400 K. Tick marks indicate the positions of allowed Bragg reflections. The difference line, observed minus calculated, is located at the bottom of the figure.

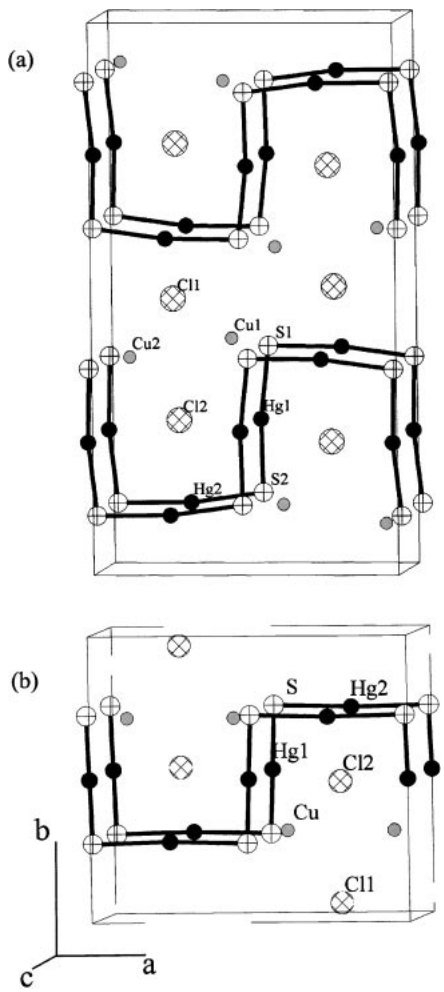

Fig. 3. Crystal structure of (a) low-temperature phase reported by Beck et al. and (b) high-temperature phase at 400 K for CuHgSCl.

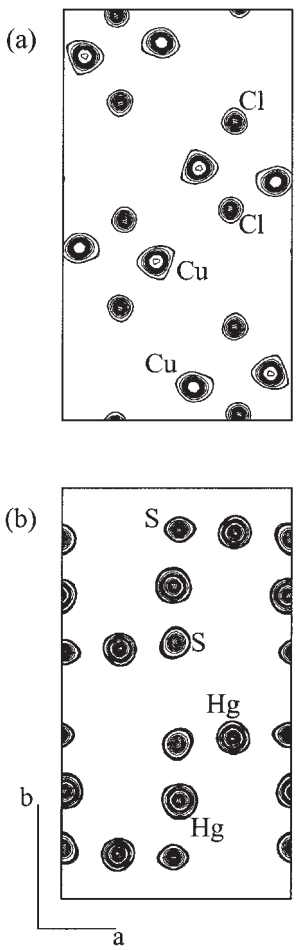

Fig. 4. The charge density maps determined by MEM along (001) plane for CuHgSCl at room temperature (a) at Cu–Cl plane and (b) at Hg–S plane. The contour lines are drawn (a) from 5.0 to 240.0 e $Å^{-3}$ and (b) from 5.0 to 1200.0 e $Å^{-3}$ at log scale intervals, respectively.

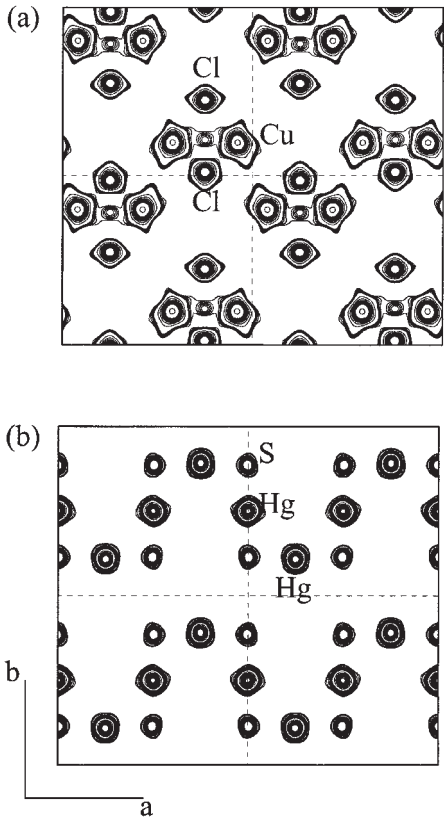

Fig. 5. The charge density maps determined by MEM along (001) plane for CuHgSCl at 500 K (a) at Cu–Cl plane and (b) at Hg–S plane. Both planes display four unit cells. The contour lines are drawn (a) from 5.0 to 240.0 e $Å^{-3}$ and (b) from 5.0 to 1200.0 e $Å^{-3}$ at log scale intervals, respectively.

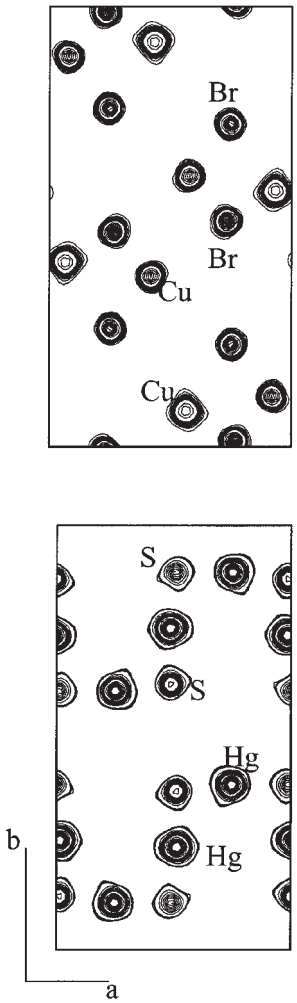

Fig. 6. The charge density maps determined by MEM along (001) plane for CuHgSBr at room temperature (a) at Cu–Br plane and (b) at Hg–S plane. The contour lines are drawn (a) from 5.0 to 240.0 e $Å^{-3}$ and (b) from 5.0 to 1200.0 e $Å^{-3}$ at log scale intervals, respectively.

transport number values using ion-blocking method revealed that the electronic contribution to the conduction process is about 10%, in comparison with about 90% of the Cu^+ ionic contribution. Ionic transport number (t_{ion}) of the sample was examined using the relation $t_{ion} = I_{ion}/I_t$, where I_{ion} is the current due to the mobile ions and I_t is the total current due to all the mobile species.

Discussion

DTA. We observed a reversible phase transition with no thermal hysteresis at 373 K for CuHgSCl and at 346 K for CuHgSBr. The crystal structure reported by Beck et al.[4] corresponds to the low temperature phase. These findings indicate that the phase transitions observed in both compounds are of second order. Thus the space group of the low temperature phase should be a subgroup of the high temperature phase. This will be described below.

Crystal Structure of High Temperature Phase for CuHgSCl. The space group notation *Pmam* was used here, which is different from *Pmma* (No. 51), because the length of *b*-axis in the high temperature phase is half of that in the low temperature phase. The lengths of *a*- and *c*-axes are unchanged. Moreover, *Pmam* belongs to a subgroup of *Pbma* that is consistent with the above estimation. Hg and S are located in the $z = 0$ plane and form zig-zag chains along *a*-axis. On the other hand, Cu and Cl are located in the $z = 1/2$ plane. Cu is surrounded by S and Cl, and is set in the center of a CuS_2Cl_2 tetrahedra. As shown in Fig. 3, the atomic positions were not changed so much. This finding also satisfies a displacive-type phase transition.

Ionic Conductivity and the Mechanism. As shown in Fig. 8, the conductivity for CuHgSCl was higher than that of CuHgSBr. The activation enthalpy is obtained from the following equation.[9]

$$\sigma(T) = \sigma_0 \exp(-\Delta H/RT), \quad (1)$$

where σ is the electric conductivity. By fitting Eq. 1 to the observed data, the activation enthalpy ΔH was evaluated to be 53 kJ mol^{-1} for CuHgSCl and 67 kJ mol^{-1} for CuHgSBr. These ΔH values would correspond to the Cu motion and the formation for defects, since all Cu sites in CuHgSX are completely occupied.[9]

We tried to identify the motion of the Cu^+ ion using ^{63}Cu NMR, but failed to detect the signal, due probably to large quadruple interaction of Cu. Therefore, the evidence has been obtained from the comparison of the charge density maps of

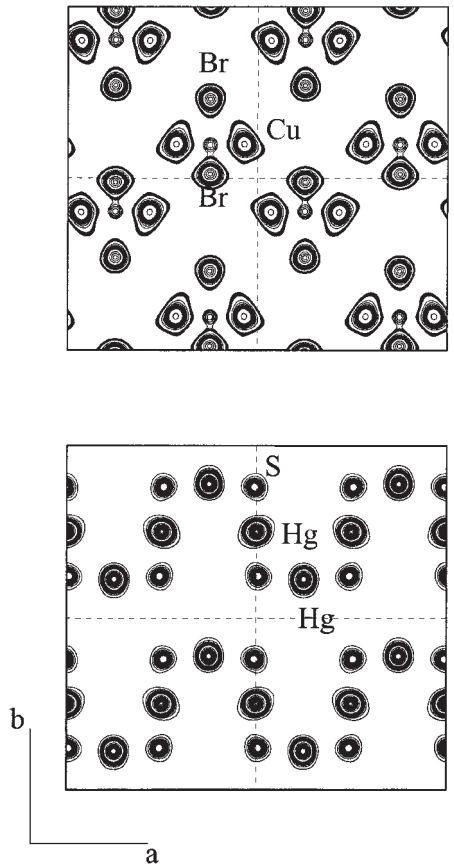

Fig. 7. The charge density maps determined by MEM along (001) plane for CuHgSBr at 500 K (a) at Cu–Br plane and (b) at Hg–S plane. Both planes display four unit cells. The contour lines are drawn (a) from 5.0 to 240.0 e $Å^{-3}$ and (b) from 5.0 to 1200.0 e $Å^{-3}$ at log scale intervals, respectively.

CuHgSCl at room temperature and at 500 K. As shown in Fig. 4, the density distribution on each atom is clearly localized. This indicates that all atoms are static at room temperature. However, in Fig. 5, the clear overlap of electron densities between the neighboring Cu atoms at 500 K show the presence of ionic conduction, although the electron densities on Cl, Hg and S atoms are still localized. Therefore, Cu atoms transfer along the (100) direction, and it can be concluded that CuHgSCl is an ionic conductor.

For CuHgSBr, the similar consideration can be applied, as shown in Figs. 6 and 7. Hence, CuHgSBr is also an ionic conductor, which has the same conduction mechanism as CuHgSCl has. We showed in the previous section that the ionic conductivity for CuHgSBr is lower than that for CuHgSCl. The presence of bigger Br ion leads to a shrinkage of the bottle-neck of the conduction path.

Conclusion

CuHgSX (X = Cl and Br) show the ionic conduction phase accompanied by the second-order phase transition at 373 and 346 K, respectively. The unit cell in the high temperature phase is halved compared with that in the low temperature one. The ionic conductions of CuHgSX (X = Cl, Br) were carried out by Cu^+ ion jumping to the neighboring Cu sites along (100) direction. The Cu^+ ion motion and the formation of defects need 53 kJ mol^{-1} for CuHgSCl and 67 kJ mol^{-1} in CuHgSBr. The conductivity of CuHgSCl appears higher than CuHgSBr, since bigger Br blocks the Cu^+ ion conduction path.

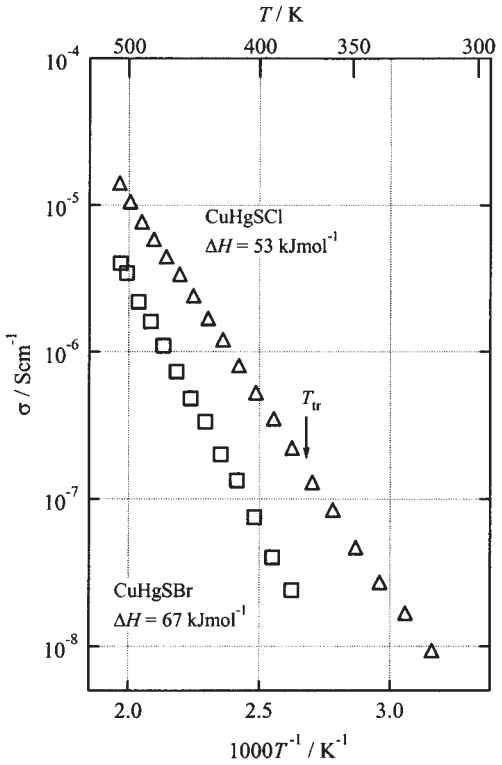

Fig. 8. Temperature dependence of electric conductivity in CuHgSX (X = Cl, Br).

References

1 M. Guillo, B. Mercey, and A. Deschanvres, *Mater. Res. Bull.*, **14**, 947 (1979).

2 R. Blachnik and H. A. Dreisbach, *Monatsh. Chem.*, **117**, 305 (1986).

3 R. Blachnik and K. Lytze, *Thermochim. Acta*, **190**, 79 (1990).

4 J. Beck, H. Keller, M. Rompel, and L. Wimbert, *Z. Anorg. Allg. Chem.*, **627**, 2289 (2001).

5 J. Beck and M. Rompel, *Z. Anorg. Allg. Chem.*, **629**, 421 (2003).

6 H. Miura and T. Kikuchi, *J. Chem. Software*, **5**, 163 (1999).

7 F. Izumi, "The Rietveld Method," ed by R. A. Young, University Press, Oxford (1993), pp. 236–253.

8 F. Izumi, *Rigaku J.*, **17**, 34 (2000).

9 S. Chandra, "Superionc Solid, Principles and Applications," North-Holland Pub. Co., Amsterdam (1981), p. 225.